THE JOURNAL OF PHYSICAL CHEMISTRY B

ARTICLE

pubs.acs.org/JPCB

Simulating pH Titration of a Single Surfactant in Ionic and Nonionic Surfactant Micelles

Brian H. Morrow,[†] Yuhang Wang,[†] Jason A. Wallace,[†] Peter H. Koenig,[§] and Jana K. Shen*[,†,‡]

[†]Department of Chemistry and Biochemistry, and [‡]School of Chemical, Biological and Materials Engineering, University of Oklahoma, Norman, Oklahoma, United States

[§]Computational Chemistry, Modeling & Simulation GCO, Procter and Gamble, Cincinnati, Ohio, United States

Supporting Information

ABSTRACT: Calculation of surfactant pK_a's in micelles is a challenging task using traditional electrostatic methods due to the lack of structural data and information regarding the effective dielectric constant. Here we test the implicit- and hybrid-solvent-based continuous constant pH molecular dynamics (CpHMD) methods for predicting the pK_a shift of a lauric acid solubilized in three micelles: dodecyl sulfate (DS), dodecyltrimethylammonium (DTA), and dodecyltriethylene glycol ether (DE3). Both types of simulations are able to reproduce the observed positive pK_a shifts for the anionic DS and nonionic DE3 micelles. However, for the cationic DTA micelle, the implicit-solvent simulation fails to predict the direction of the pK_a shift, while the hybrid-solvent simulation, where conformational sampling is conducted in explicit solvent, is consistent with experiment, although the specific-ion effects remain to be accurately determined. Comparison between the implicit- and hybrid-solvent data shows that the latter gives a more realistic description of the conformational environment of the titrating probe. Surprisingly, in the DTA micelle, surfactants are only slightly attracted to the laurate ion, which diminishes the magnitude of the electrostatic stabilization, resulting in a positive pK_a shift that cannot be explained by chemical intuition or other theoretical models. Our data underscores the importance of microscopic models and ionization-coupled conformational dynamics in quantitative prediction of the pK_a shifts in micelles.

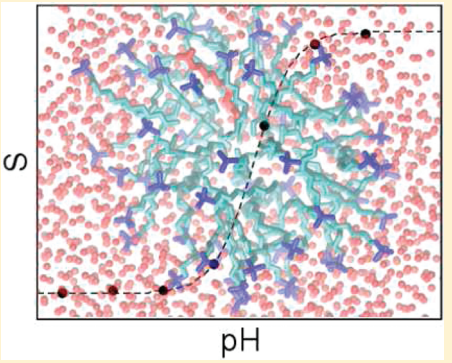

1. INTRODUCTION

Surfactants are amphipathic molecules consisting of a hydrophilic (polar or ionic) headgroup and a hydrophobic tail (typically a long hydrocarbon chain). Because of the presence of both hydrophilic and hydrophobic parts, surfactants exhibit unusual properties such as accumulation at various liquid interfaces and self-association to form micelles in aqueous solutions above the critical micelle concentration (cmc).[1,2] Surfactants are found in detergents, cosmetics, paints, plastics, food, and pharmaceuticals. They are also used in oil recovery and environmental remediation of contaminants.[1] Because of the wide range of applications, considerable effort has been made to understand thermodynamics of the formation and stability of surfactant micelles using experimental techniques[3,4] and theories.[5−10]

On the basis of the net charge of the hydrophilic headgroup, surfactants are classified as nonionic, cationic, anionic, and zwitterionic or amphoteric. Above the cmc and at a given temperature and salt concentration, the phase behavior and micellar morphology of ionic and amphoteric surfactant systems vary strongly with pH conditions.[11] For example, fatty acids such as the 12-carbon lauric acid, also known as dodecanoic acid, H_3C-$(CH_2)_{10}$-COOH, form a lamellar phase or bilayers (vesicles) at intermediate pH conditions when both charged and neutral species are present, while at high pH conditions they form micelles.[12,13] The ratio of the charged and neutral forms of the surfactant also affects micellar size and shape, as for instance shown for the amphoteric alkyldimethylamine oxides C_{12}DAO and C_{14}DAO.[14] The effect of pH on the phase and morphological behavior of surfactants arises from the change in the ionization state of the surfactant headgroup which, in turn, affects the electrostatic potential at the micelle−water interface. A typical method to determine the mean interfacial electrostatic potential is to incorporate a probe molecule such as an acid−base indicator dye[15,16] or a titratable surfactant such as lauric acid[17] into the micelle of interest. The probe pK_a is directly related to the interfacial potential ϕ via the relationship,[18,19] $pK_a^{app} = pK_a^0 - F\phi/2.31RT$, where F is the Faraday constant and pK_a^0 refers to the intrinsic interfacial pK_a, which is commonly assumed to be the probe pK_a in a nonionic micelle. Thus, the pK_a shift, $pK_a^{app} - pK_a^0$, of the solubilized probe reports on the interfacial electrostatic environment in a charged micelle relative to a neutral one.

Despite the importance of pH titration properties of ionic micelles, relatively few theoretical models or methods have been developed.[17,20−24] In an early work by Mille, analytical expressions were derived based on nearest-neighbor interaction energies

Received: July 4, 2011
Revised: November 2, 2011
Published: November 03, 2011

on a lattice.[20] It was found that charge−charge interactions alone are insufficient to reproduce the experimental titration data. More recently, regular solution theory (RST) has been applied by Maeda[22] and by Blankschtein and Goldsipe[23] to predict the pK_a's of titratable or pH-sensitive surfactants in micelles. In the latter work, the cmc's of the protonated and deprotonated forms of the titratable surfactant and pairwise interaction parameters were used to quantify the pK_a shifts of pH-sensitive surfactants solubilized in nontitratable (pH-insensitive) micelles relative to the monomer pK_a in solution.[23] Although RST-based empirical modeling offers quantitative predictions, it requires significant experimental efforts to determine cmc's and interaction parameters, and it does not offer physical insights at the microscopic level. To address these limitations, Blankschtein and Goldsipe developed a molecular-thermodynamic theory based on minimization of the free energy of micellization which is expressed in terms of contributions of different physical origins, with respect to the variables that represent micellar shape, size, concentration of counterions, and composition.[10,25] For a solubilized pH-sensitive probe in the micelle, the theory gave accurate prediction for the pK_a shift of C_{12}DAO in the nonionic micelle of dodecyloctaethylene glycol ether ($C_{12}E_8$ or DE8) and for the anionic micelle of sodium dodecyl sulfate (SDS) but not for the cationic micelle of dodecyltrimethylammonium bromide (C_{12}TAB, DoTAB or DTAB). In the latter case, compared to the experimental shift of −0.8 to −0.9, the prediction was about 2 pK units too low.[25] This means the positively charged environment of DTA is not as destabilizing for the protonated form of the probe molecule, $C_{12}DAOH^+$, as the theory predicts.

In a study by da Silva and co-workers, Poisson−Boltzmann (PB) calculations and Monte Carlo (MC) simulations based on a spherical cell model with low and high dielectric regions were used to predict and rationalize the observed pK_a shifts of a probe lauric acid (relative to the solution value) in SDS, DE8, DTAC (dodecyltrimethylammonium chloride), and DTAB micelles.[17] Both PB calculations and MC simulations were able to qualitatively reproduce the positive pK_a shift in the anionic SDS micelle. By increasing the radius of the low dielectric cavity, which represents the hydrophobic core of the micelle, MC simulations were also able to capture the positive pK_a shift in the neutral DE8 micelle. However, none of the theoretical approaches can predict the positive shifts in the cationic DTAC and DTAB micelles. In fact, a positive pK_a shift in cationic micelles is counterintuitive, since the positive charges of DTA molecules provide stabilization for the laurate ion, also known as the soap or ionized form of lauric acid. Nonetheless, it is reminiscent of the small negative pK_a shift of C_{12}DAO, which has a solution pK_a of 4.9, similar to lauric acid, in the DTAB micelle, which could not be reproduced by the thermodynamic theory.[25] Intrigued by these studies, we sought to develop simulation approaches that can offer quantitative estimates of pK_a shifts for a single surfactant solubilized in ionic and neutral micelles with microscopic insights.

The calculation of micellar pK_a's that includes atomically detailed interactions is a nontrivial task. Poisson−Boltzmann-based methods, widely used in pK_a calculations for proteins, are not applicable because of several difficulties. First, micelle structures are not available. Second, an effective dielectric constant for describing the micellar environment is not known. The continuous constant pH molecular dynamics (CpHMD) method[26,27] with the generalized-Born (GB) implicit-solvent model GBSW[28] and temperature replica-exchange (REX) sampling protocol,[29] on the other hand, does not require high-resolution structure input because proton titration is directly coupled to conformational dynamics as demonstrated in studies of pH-dependent protein folding.[30−32] Furthermore, the CpHMD method does not rely on an effective dielectric constant because the local dielectric response arises naturally from microscopic structural rearrangement. Benchmark studies showed that short-time (up to 1 ns) REX-CpHMD simulations starting from X-ray structures or NMR models offer pK_a predictions with a root-mean-square deviation (rmsd) below 1 pK units for surface and moderately buried side chains in proteins.[29,33] The most recent blind prediction of pK_a's for deeply buried side chains in the mutants of staphylococcal nuclease based on 500 ps sampling (per replica) gave an rmsd of 1.69 pH units.[34]

The objective of this work is to evaluate whether the GB-based CpHMD titrations can be used to quantitatively predict the pK_a of a probe lauric acid solubilized in the anionic DS, cationic DTA, and nonionic DE3 micelles. We will make use of a recently parametrized GBSW model for surfactant simulations.[35] We will also test the newly developed hybrid explicit/implicit-solvent based CpHMD method,[36] which is more accurate than the GB-based method, and apply it to delineate microscopic origins of the observed pK_a shifts. The predicted pK_a shifts are in good agreement with experiment. Our data reveals a tight coupling between protonation−deprotonation equilibrium of the probe molecule and its conformational dynamics in the micellar environment.

2. SIMULATION METHODS AND PROTOCOLS

Simulation Methods. To facilitate later discussions, we give a brief description of the continuous constant pH molecular dynamics (CpHMD) method, which is what the current study is based on. Full details can be found elsewhere.[26,27] In CpHMD, a titration coordinate, λ, is introduced for each group that can change protonation state. The titration coordinates are propagated along with the atomic coordinates using an extended Hamiltonian formalism

$$\mathscr{H}(\{\mathbf{r}_a\},\{\boldsymbol{\theta}_i\}) = \sum_a \frac{m_a}{2}\dot{\mathbf{r}}_a^{\,2} + U^{\mathrm{int}}(\{\mathbf{r}_a\}) + \sum_i \frac{m_i}{2}\dot{\boldsymbol{\theta}}_i^{\,2} + U^{\mathrm{hybr}}(\{\mathbf{r}_a\},\{\boldsymbol{\theta}_i\}) + U^{*}(\{\boldsymbol{\theta}_i\}) \quad (1)$$

where a is the index for atomic coordinates and i is the index for the continuous variables θ_i, which are related to the titration coordinates λ_i by $\lambda_i = \sin^2(\theta_i)$. While the value of θ_i is unrestricted, λ_i is bound between 0 (protonated) and 1 (unprotonated). For groups with two protonation sites such as the carboxyl oxygens in lauric acid, an additional coordinate for tautomer interconversion is introduced. This two-dimensional titration coordinate is indicated by bold $\boldsymbol{\theta}$.

In eq 1, the first and third terms give the kinetic energies of atoms and fictitious λ particles, respectively. U^{int} represents the bonded potential energy, which is independent of titration coordinates. U^{hybr} represents an effective energy, which depends on both spatial and titration coordinates, thus enabling the coupling between conformational dynamics and protonation equilibria. In the original formulation of the CpHMD method, which is based on the generalized Born (GB) implicit-solvent model, U^{hybr} is a sum of van der Waals, Coulombic, and electrostatic solvation free energies. The latter can be written in

terms of self-solvation energies and solvent dielectric screening of Coulombic interactions

$$\Delta G_{solv} = -\frac{1}{2}\sum_{a}\left(1-\frac{e^{-\kappa\alpha_a}}{\varepsilon_w}\right)\frac{{q_a}^2}{\alpha_a}-\frac{1}{2}\sum_{a\neq b}\left(1-\frac{e^{-\kappa f_{GB}}}{\varepsilon_w}\right)\frac{q_a q_b}{f_{GB}} \quad (2)$$

Here q_a and q_b are the respective partial atomic charges of atoms a and b, and ε_w is the dielectric constant of water. The Debye−Hückel term $e^{-\kappa f_{GB}}$, where $\kappa^2 = 8\pi q^2 I/ek_bT$, r_{ab} is the distance between atoms, and I is the ionic strength, is used to approximately account for the effect of salt screening. The term f_{GB} is defined as

$$f_{GB} = \sqrt{{r_{ab}}^2 + \alpha_a\alpha_b \exp(-{r_{ab}}^2/4\alpha_a\alpha_b)} \quad (3)$$

where r_{ab} is the distance between atoms and α_a and α_b are the effective Born radii.

GB implicit-solvent models are efficient[37] and offer accurate estimates of the electrostatic solvation energies.[38] However, several molecular dynamics simulation studies revealed inherent limitations in conformational sampling based on GB models. For example, hydrogen bonding is too strong and hydrophobic assemblies such as unfolded proteins and surfactant micelles are too compact and rigid.[39,35] These limitations manifest in CpHMD simulations as pronounced deviations between the calculated pK_a's and experimental data.[39,36] To improve the representation of conformational states, we have recently extended the CpHMD method for explicit-solvent simulations.[36] In this new method, which we will refer to as the hybrid-solvent CpHMD, conformational dynamics of the solute are propagated using the explicit-solvent model, while solvent-modulated forces on the titration coordinates are efficiently evaluated using the GB model to allow rapid convergence. Details of the hybrid-solvent CpHMD method can be found in our recent work.[36] In this paper, we have performed titration simulations using both implicit- and hybrid-solvent based CpHMD methods.

Simulation Protocols. Three C_{12} surfactant micelles were studied here (Figure 1): an anionic micelle composed of dodecyl sulfate (DS), a cationic micelle composed of dodecyltrimethylammonium (DTA), and a nonionic micelle composed of dodecyltriethylene glycol ether (DE3). A probe lauric acid was substituted for one of the DS, DTA, or DE3 molecules. For consistency, an aggregation number of 60 was used for all of the micelles. Although the measured aggregation numbers vary somewhat depending upon experimental techniques and solution conditions, 60 is a good approximation for all three micelles at low surfactant concentrations.[40−43] This aggregation number has also been used in previous simulations which reproduce experimental data.[44,45] Another reason for using 60 is that the ratio between surfactant molecules and solubilized lauric acid was about 60 in the experiment that determined the pK_a shift of lauric acid in the DS, DTA, and DE8 micelles.[17] The three micelles were constructed from the C_{60} buckminsterfullerene model following the procedure of MacKerell.[44] For the hybrid-solvent simulations, the starting structures were solvated in an octahedral water box with 60 sodium and chloride counterions added to the DS and DTA micelles, respectively. The solvated systems then underwent energy minimization using 50 steps of steepest descent minimization followed by 150 steps of adopted basis Newton−Raphson calculation.

All simulations were conducted using a developmental version of CHARMM (c35b3),[46] where both the GB and hybrid-solvent-based CpHMD methods are implemented.[27,36] The surfactant molecules are represented by the CHARMM27 lipid force field.[47,48] The parameters for the sulfate headgroup of DS were the same as in methyl sulfate. The parameters for the headgroup of DTA (trimethylammonium) were the same as in phosphatidylcholine. The parameters for the headgroup of DE3 (triethylene glycol ether) were taken from ref 49. The GB implicit-solvent model with a simple switching function (GBSW)[28] was used. The GB input radii for the surfactant molecules were recently parametrized using a procedure based on the radial distribution functions of solvent charge density and adjustment to match potentials of mean force from the simulations in explicit solvent.[35] The nonpolar surface tension coefficient was set to 0.03 kcal/(mol·Å^2), consistent with the validation study using the same set of GB input radii.[35] For the hybrid-solvent CpHMD simulations, the TIP3P water model[50] was used in conformational sampling. Unless otherwise specified, an ionic strength of 0.15 M was used in the GB electrostatics calculations, consistent with the value used in the parametrization of GB input radii for DS, DTA, and DE3 surfactants.[35] In the Monte Carlo simulations of SDS and DTAC using a Yukawa/Debye−Hückel potential to model salt screening, Jusufi et al. found that ionic strengths below 0.15 M failed to reproduce the experimental aggregation number.[51]

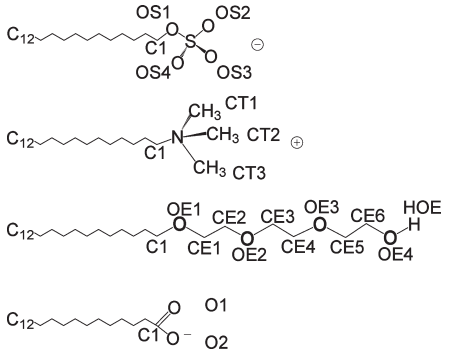

Figure 1. Surfactant molecules studied in this work. From top to bottom: dodecyl sulfate (DS), dodecyltrimethylammonium (DTA), dodecyltriethylene glycol ether (DE3), and lauric acid. Atoms are named according to the convention in the CHARMM force field.[47,48,56]

To enhance sampling of protonation and conformational states and accelerate convergence of pK_a values, two types of replica-exchange (REX) sampling protocols were applied (as implemented in the MMTSB toolset[52]). The GB-based titration simulations were carried out at a single pH and multiple temperatures with the temperature-based REX (T-REX) protocol,[29] which included 12 replicas occupying the exponentially spaced temperature windows ranging from 298 to 350 K. Two adjacent temperature replicas were allowed to exchange spatial and titration coordinates every 1.0 ps based on the Metropolis criterion.[29] The simulation length for each replica was 500 ps, which is consistent with previous work[29,34] (see more discussions in Results and Discussion), resulting in a total of 6 ns for a set of REX simulations. For analysis, the replica at 298 K was used with the data from the first 100 ps being discarded. For the DS micelle, the T-REX simulations were performed at pH 7 and 8. For the DTA and DE3 micelles, the T-REX simulations were performed at pH 2 and 6.5, respectively. The T-REX simulations were repeated four times to obtain standard deviations for the calculated pK_a value. Other details of GB-based T-REX titration simulations can be found in the previous work.[29]

Table 1. Calculated and Experimental pK_a Shifts of Lauric Acid in the Anionic, Cationic and Nonionic Micelles

		explicit solvent[a]		
	implicit solvent[a]			
micelle	0.15 M	0.15 M	0 M	experiment[b]
DS	2.5 ± 0.33	3.2 ± 0.02	5.3	2.8 ± 0.1 (SDS)
				2.8 ± 0.1 (LiDS)
DTA	−3.0 ± 0.06	1.5 ± 0.01	0.6	0.1 ± 0.1 (DTAC)
				0.9 ± 0.1 (DTAB)
DE3	1.6 ± 0.26	1.7 ± 0.09	1.5	1.9 ± 0.1 (DE8)

[a] Calculated average pK_a's with standard deviations. The ionic strengths used in the calculation of GB solvation energies are given. pK_a shifts are relative to the model value of 5.0 (see Simulation Methods and Protocols). [b] Experimental data were collected at a weight fraction of 5%,[17] which is well above the cmc values of all three micelles. pK_a shifts are relative to the solution pK_a of 4.8 for acetic acid measured using the same technique.[17] The measured pK_a's are very similar to those reported later by Söderman et al.[24]

The hybrid-solvent titration simulations were carried out at 298 K and multiple pH values with the pH-based replica exchange (pH-REX) protocol.[36] The pH-REX protocol was used because T-REX is ineffective for conformational sampling in explicit solvent due to the requirement of a large number of replicas. The pH-REX protocol used here included seven replicas with 1 pH unit spacing and in the pH range of 4.5−10.5 for DS, 4−10 for DTA, and 3.5−9.5 for DE3 micelles. An exchange of pH conditions between two adjacent replicas was attempted every 1.0 ps according to the Metropolis criterion. The simulation length for each replica was 2 ns, resulting in a total simulation time of 14 ns for each set of REX simulations. The final 1 ns was used for analysis. Two independent pH-REX simulations were carried out to estimate the uncertainty in the calculated pK_a's. For the DTA micelle, four independent pH-REX simulations were carried out. Other simulation details can be found in a recent work.[36]

To determine the parameters in the potential of mean force (PMF) function for titrating an isolated lauric acid using the GB and hybrid-solvent CpHMD simulations, thermodynamic integration was performed as described in the previous work.[27,36] The model compound pK_a used was 5.02, which is the pK_a of lauric acid found in high dilution.[53] To verify the accuracy of the model PMF, five independent 1 ns titration simulations were performed at pH 5. The resulting pK_a's from the GB and hybrid-solvent simulations were found to be 5.0 ± 0.06 and 4.9 ± 0.11, respectively, in excellent agreement with the target value. The pK_a of lauric acid was obtained by fitting the unprotonated fractions (S) to the Hill equation

$$S = \frac{1}{1 + 10^{n(\mathrm{p}K_a - \mathrm{pH})}} \quad (4)$$

where n is the Hill coefficient.

3. RESULTS AND DISCUSSION

3.1. GB-Based Titration Simulations. *Calculated pK_a Values of Lauric Acid in the Micelle.* We conducted four independent sets of T-REX titration simulations of DS, DTA, and DE3 micelles containing a titratable lauric acid in GB implicit solvent. Each set of REX simulations utilized 12 replicas and lasted 500 ps per replica, resulting in the total simulation time of 6 ns. We adopted the simulation length of 500 ps per replica based on our previous benchmark work and blind prediction exercise, which demonstrated that sampling of 500 ps per replica is sufficient for obtaining converged pK_a values for solvent-exposed and moderately buried residues in proteins of various sizes.[29,33,34] Prolonged simulations would likely worsen the pK_a predictions because of limitations in the GB model which result in the overly compact and rigid micelles as observed in a related study.[35]

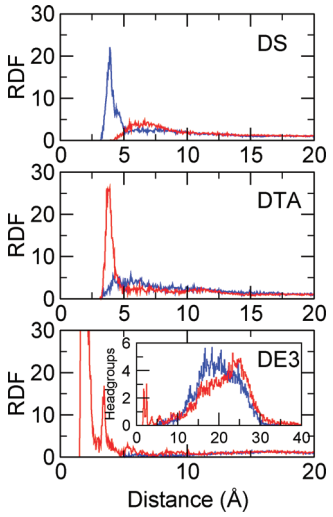

Figure 2. Radial distribution function between the headgroups of lauric acid and surfactant monomers obtained from the GB-based titration simulations. The distance is measured from the center of mass of the carboxylate oxygens in lauric acid and a headgroup atom in the surfactant (sulfur in SDS, nitrogen in DTA or hydroxyl hydrogen in DE3). The inset in the bottom panel shows the number of DE3 headgroups at a given distance from lauric acid. Results for the protonated and deprotonated forms of lauric acid are shown in blue and red, respectively.

The calculated pK_a shifts relative to the solution pK_a of 5.0 are given in Table 1. The standard deviations are below 0.3 pK units, on par with the typical uncertainty of 0.2 pK units in protein titration simulations.[29,33] For the anionic DS and neutral DE3 micelles, simulations resulted in positive pK_a shifts of 2.5 and 1.6, in excellent agreement with the experimental data. For the cationic DTA micelle, however, simulation gave a negative pK_a shift of −3.0, in disagreement with the experimental shifts of 0.1 and 0.9 in the presence of chlorides and bromides, respectively. To understand the origins of pK_a shifts in different micelles, we examine the interaction of lauric acid with surfactant monomers in the micelle and the solvent accessibility of the lauric acid headgroup.

Interaction of Lauric Acid with Surfactants in the Micelle. To examine the environment of the protonated (lauric acid) and deprotonated (laurate ion) forms of lauric acid in three micelles, we calculated the radial distribution function (RDF) from the carboxylate headgroup of lauric acid to the headgroups of other surfactants (Figure 2). In the anionic DS micelle, the RDF for lauric acid shows a sharp peak at 4 Å, indicating an increased probability for finding DS monomers near lauric acid. By contrast, the RDF for laurate ion is broad and has a maximum at 6−7 Å, indicating the lack of close-range interactions, as expected from the electrostatic repulsion with the negatively charged DS monomers. The opposite behavior is seen for the

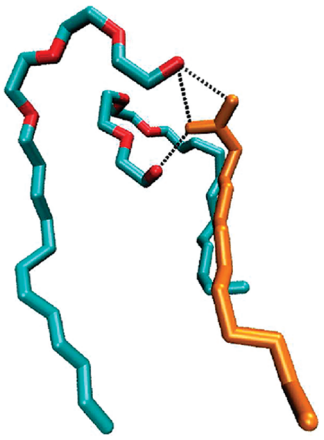

Figure 3. A representative snapshot from the GB-based simulations showing hydrogen bonding between the headgroups of laurate ion and DE3. For clarity, hydrogen atoms and other surfactants in the micelle are hidden.

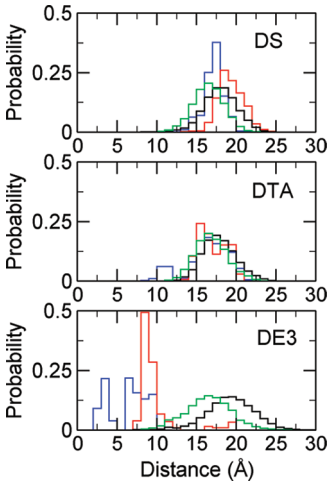

Figure 4. Distance distribution from the headgroups of lauric acid and surfactant monomers to the micellar center of mass obtained from the GB-based titration simulations. The distance is measured from the carboxylate carbon of lauric acid (blue, protonated; red, deprotonated), a headgroup atom of the surfactant in black (sulfur of SDS, nitrogen of DTA or hydroxyl oxygen of DE3), and the C1 carbon of the surfactant (green).

cationic DTA micelle. The cationic DTA headgroups are attracted to the laurate ion, leading to a sharp peak in the RDF at 4 Å, whereas the lauric acid weakly interacts with DTA monomers, resulting in a broad distribution with a maximum at 4−6 Å. The behavior of lauric acid in the neutral DE3 micelle is qualitatively different. While the RDF for the lauric acid is almost flat, indicating an absence of preferential interactions with DE3, the RDF for the laurate ion shows a disproportionally high peak in the range of 1.7−2 Å. Examination of the trajectory snapshots shows that the carboxylate of laurate ion was almost always hydrogen bonded to the hydroxyl ends of two or three DE3 molecules, which resulted in increased bending of the triethylene glycol group toward the micelle center as compared to other DE3 monomers (Figure 3). The clustering of DE3 around laurate ion can also be seen from the distribution of the distance between the

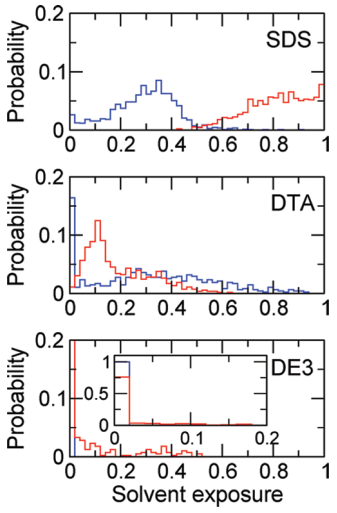

Figure 5. Probability distribution of the solvent exposure of the headgroup of lauric acid (blue, protonated; red, deprotonated) obtained from the GB simulations. Solvent exposure is defined as the ratio of the solvent-accessible surface area (SASA) of the carboxylate headgroup in the micelle and that in water in the same conformation.

carboxylate oxygens of laurate ion and hydroxyl oxygen of DE3 (Figure 2, inset in the bottom plot).

Position of Lauric Acid in the Micelle. We examine the position of the headgroup of the lauric acid and laurate ion in comparison to the headgroups of surfactant monomers. Figure 4 shows the probability distributions of the distances from the carboxylate group as well as surfactant headgroups to the center of the micelle. The latter can be used to gauge the approximate location of the micelle surface. We avoid using the term micelle−water interface because the surfactant headgroups in all three micelles, especially DE3, have significantly reduced solvent accessibility in GB as compared to the hybrid-solvent simulations.[35] We will return to this point later. Figure 4 also shows the distances from the C1 atoms of surfactant monomers to specify the location of the hydrophobic boundary in the micelle, which is somewhat farther away from the micelle surface in the DE3 micelle due to the long headgroup. In the DS micelle, while lauric acid is close to the micelle surface, laurate ion is slightly extended out to solvent, as seen from its slightly larger distance to the micelle center as compared to the DS monomers. In the DTA micelle, the headgroups of the lauric acid and laurate ion are close to the micelle surface, except that the former occasionally goes deep into the hydrophobic core of the micelle. The position of lauric acid in the neutral DE3 micelle is qualitatively different. Both the headgroups of the lauric acid and laurate ion are buried in the hydrophobic core of the micelle. The distribution for the laurate ion is narrow, reflecting the fact that it is trapped by hydrogen bonding with two or three DE3 molecules (see discussion above).

Solvent Accessibility of Lauric Acid in the Micelle. The degree of solvent exposure is another determinant for pK_a shifts in micelles. It is also correlated with the position of the lauric acid headgroup relative to the micelle surface when comparing data across the GB (or hybrid-solvent) simulations. Figure 5 shows the probability distribution of the solvent exposure of the lauric acid headgroup in the micelle. A value of 1 represents complete exposure to solvent, while a value of zero represents complete exclusion from solvent. In the DS micelle, solvent exposure of the

Table 2. Average Relative Born Radius[a] of the Carboxylate Oxygens of Lauric Acid in Micelles

micelle	implicit solvent		explicit solvent	
	protonated	deprotonated	protonated	deprotonated
DS	1.23 ± 0.20	1.08 ± 0.02	1.18 ± 0.24	1.07 ± 0.04
DTA	1.38 ± 0.46	1.23 ± 0.11	1.30 ± 0.30	1.17 ± 0.21
DE3	2.60 ± 0.67	1.68 ± 0.50	1.29 ± 0.35	1.10 ± 0.10

[a] Average relative Born radius is calculated as the average of the effective Born radii of the carboxylate oxygens of lauric acid in the micelle divided by that in water.

laurate ion and lauric acid ranges from 0.5 to 1, and 0 to 0.5, respectively. Thus, deprotonation of lauric acid leads to greater solvent exposure, consistent with the observation that laurate ion is slightly extended outside of the DS micelle (Figure 4). Surprisingly, Figure 5 shows that both lauric acid and lauric ion can rarely gain access to solvent in the DTA micelle. While the neutral lauric acid is most of the time completely buried, the distribution of solvent exposure of the laurate ion peaks at 0.1, which indicates that deprotonation does not significantly increase solvent exposure. Since the carboxylate carbon in both the neutral and charged forms of lauric acid is most of the time located at the level of C1 atoms of DTA (Figure 4), low solvent accessibility likely results from the drastically reduced mobility and solvation of surfactants in the DTA micelle in GB solvent, as shown in our previous work.[35] Lastly, in the DE3 micelle, both the lauric acid and laurate ion are completely excluded from solvent, consistent with the previous observation that both forms of lauric acid mainly explore the hydrophobic region of the micelle.

The effective Born radius of an atom represents the distance to the dielectric boundary when considering the solute as a sphere. It is a central quantity in GB models, because it determines the self-solvation energy and the degree of solvent screening of Coulombic interactions (see eq 2). As lauric acid becomes buried from water, the effective Born radii increase, resulting in a decrease of the self-solvation energy which contributes to a positive pK_a shift (see more discussions later). Table 2 summarizes the average relative Born radius of the carboxylate oxygens in the DS, DTA, and DE3 micelles with respect to the value in water. In the DS micelle, the relative Born radius decreases from 1.23 to 1.08 upon deprotonation, in agreement with the significant increase in the solvent exposure of the laurate ion as it moves slightly outside of the micelle−water interfacial region. In the DTA micelle, the relative Born radii for the neutral lauric acid and laurate ion are 1.38 and 1.23, respectively, which are larger than the corresponding values in the DS micelle, consistent with the fact that the carboxylate headgroup, especially the ionized form, becomes more buried. In the DE3 micelle, the relative Born radii for the lauric acid and laurate ion are 2.60 and 1.68, significantly larger than those in the ionic micelles, reflecting the fact that both forms are completely buried in the hydrophobic core of the micelle.

3.2. Hybrid-Solvent-Based Titration Simulations. Recently, we have compared the conformational dynamics of the DS, DTA, and DE3 micelles in the GB implicit-solvent and explicit-solvent simulations.[35] We found that the micelles in implicit solvent are more compact and rigid than those in explicit solvent. A less realistic description of the conformational dynamics of micellar surfactants could affect the electrostatic environment around the titrating headgroup of lauric acid, resulting in inaccurate pK_a calculations. These observations, combined with the poor pK_a prediction for the DTA micelle, led us to perform titration simulations using the hybrid-solvent CpHMD method where conformational sampling is performed in explicit solvent. While more computationally expensive, these simulations are expected to provide more consistently accurate pK_a calculations as shown in our recent study of protein titrations due to the more accurate representation of native-state structures, hydrophobic clusters, and solvent-mediated charge−charge interactions.[36]

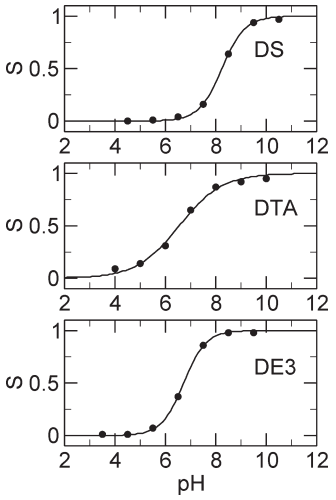

Figure 6. Titration curves for lauric acid in the SDS, DTA, and DE3 micelles from the explicit-solvent-based titration simulations. *S* is the unprotonated fraction of lauric acid. The circles and solid curves represent the data from the titration simulations and the corresponding fits to the Hill equation (eq 4), respectively.

Calculated pK_a Values of Lauric Acid in the Micelle. We performed two independent sets of pH-REX titration simulations of DS, DTA, and DE3 micelles containing a titratable lauric acid using the hybrid-solvent CpHMD. Each set of REX simulations utilized 7 pH replicas and lasted 2 ns per replica. The unprotonated fractions (*S*) in all three micelles stabilized after 500 ps to 1 ns, in agreement with the findings from the protein titration simulations using the same method.[36] Interestingly, Bruce et al. found that 1 ns is the time that was needed to achieve a converged distribution of counterions in the explicit-solvent simulation of a 60-mer DS micelle.[45]

The calculated pK_a shifts in the three micelles relative to the solution value are listed in Table 1. Two ionic strengths were used. We focus on the data obtained at 0.15 M first. The maximum deviation resulting from two sets of simulations is 0.09, suggesting a very small random error. Figure 6 shows excellent fitting of the unprotonated fractions at different pH (titration curves) to the Hill equation, which is another indication of the convergence of protonation-state sampling. Comparing the calculated pK_a shifts with experiment, quantitative agreement is found for all three micelles. For the anionic DS micelle, simulation overestimated the pK_a shift by 0.4 units. For the DE3 micelle, the calculated shift is 0.2 units lower than the measured value in the DE8 micelle. For the DTA micelle, the calculated shift is larger by 0.6 or 1.4 units, as compared to the measured value in the presence of bromides or chlorides, respectively. To understand the effects due to dielectric screening by mobile ions, we also carried out titration simulations at zero

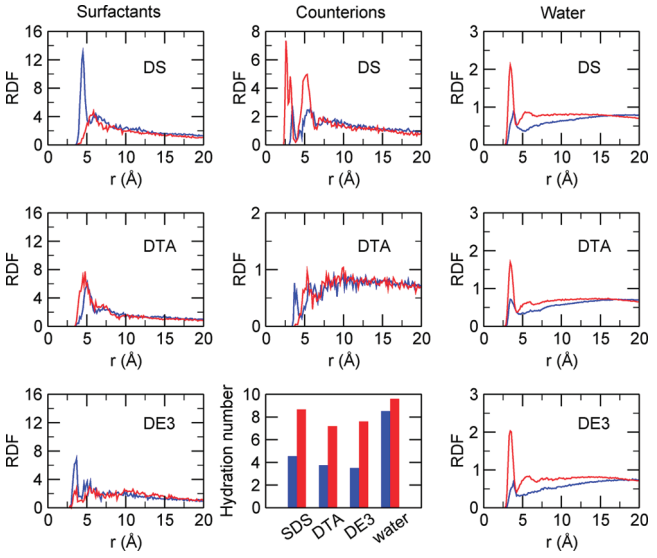

Figure 7. Radial distribution functions between the headgroup of lauric acid (measured from the carboxyl carbon atom) and surfactant headgroups (left column), counterions (center column), and water oxygen atoms (right column). Distances to DS, DTA, and DE3 headgroups are measured from the sulfur, nitrogen, and hydroxyl oxygen atoms, respectively. Bottom, center: average hydration number of lauric acid in the micelle and water. The hydration number is defined as the number of water oxygens within 4.5 Å of the carboxylate carbon atom. Results for the protonated and deprotonated lauric acid are shown in blue and red, respectively.

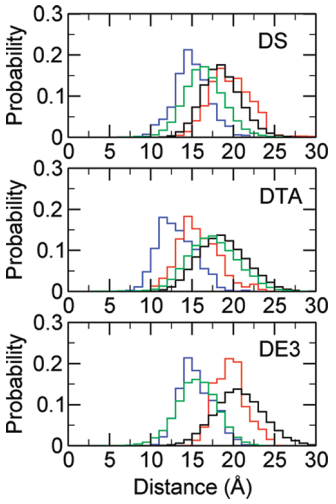

Figure 8. Distance distribution from the headgroups of lauric acid and surfactant monomers to the micellar center of mass obtained from the explicit-solvent simulations. The distance is measured from the carboxylate carbon of lauric acid (blue, protonated; red, deprotonated), a headgroup atom of the surfactant (sulfur of SDS, nitrogen of DTA or hydroxyl oxygen of DE3) in black, and the C1 carbon of the surfactant in green.

ionic strength. The change in the calculated pK_a shift is the largest for the DS micelle (2.1 units), followed by the DTA (−0.9 units), and DE3 (−0.2 units) micelles.

From Figure 6 we can see that, while the Hill coefficient for the titration curves of the DS and DE3 micelles is close to 1 as expected, it is not the case for the DTA micelle. We believe that the deviation from the standard Henderson−Hasselbalch (HH) behavior is likely the result of the slow exchange between two distinct conformational states of the lauric acid (buried in the micelle versus interfacial) relative to the time scale of simulation. Both states titrate with significantly different microscopic pK_a's. If the exchange between these two states is sampled sufficiently, e.g., equilibrium is established, the standard HH titration with one macroscopic pK_a should be observed. However, due to the slow interconversion between these two states and limited sampling time, the equilibrium is not fully established. In other words, the protonation equilibria of the two states are not fully coupled, although the individual protonation equilibrium is well converged (Figure S1 in the Supporting Information), giving rise to the deviation from the standard HH behavior. This deviation can be accounted for by fitting the titration data to a Hill equation (Figure 6) or to a two-step model based on the linear combination of two HH equations, yielding two pK_a values, 7.4 and 6.2 (Figure S2 in the Supporting Information), which represent the buried and interfacial states, respectively. Fitting to the Hill equation gives a small Hill coefficient and a macroscopic pK_a of 6.5, which is closer to the microscopic pK_a of the interfacial state, reflecting the fact that latter state is dominating as seen from the larger coefficient in the linear combination (Supporting Information). This phenomenon is only seen for the DTA micelle because, as we showed previously,[35] the DTA micelle is the most diffuse among all three micelles, and as a result the conformational change between the buried and interfacial states is most pronounced and likely slower.

Interaction of Lauric Acid with Surfactants in the Micelle. In analogy to our discussions in the context of the GB-based titration simulations, we examine the environment of the protonated and deprotonated forms of the carboxylate headgroup of lauric acid in the three micelles. The left panel of Figure 7 shows the RDFs from the carboxylate of lauric acid and laurate ion to the headgroups of surfactant monomers. In the DS micelle, the distributions of surfactant monomers around lauric acid are similar to those in the GB simulation. The neutral lauric acid tends to be in close contact with the DS headgroups as seen from the sharp peak at 4.5 Å in the RDF, while it is not the case for the negatively charged laurate ion due to electrostatic repulsion with DS. In the DTA micelle, the distributions of surfactants around lauric acid are qualitatively different from those seen in the GB simulation. Instead of showing an opposite behavior to the DS micelle, the peak position and intensity of the RDFs for the laurate ion and lauric acid are very similar, with the former being a little closer and the intensity being a little greater. Thus, in explicit solvent, the cationic DTA monomers only show a small preference for the negatively charged laurate ion, in contrast to what would be expected from the electrostatic attraction. One possible reason is that the headgroup of lauric acid spends most of the time being buried under the DTA headgroups regardless of the protonation state (Figure 8). This behavior is different from the GB simulation, where the headgroup of laurate ion is closer to the micelle surface. In the DE3 micelle, the distributions of surfactants around lauric acid are also completely different from those observed in the GB simulations. The RDFs for both protonated and deprotonated lauric acid show a peak around 3.5 Å, with the former being much stronger. The sharp peak seen for laurate ion in the GB simulation due to hydrogen bonding with DE3 monomers is absent.

Distribution of Counterions around Lauric Acid. Counterions are a feature unique to simulations in explicit solvent. The middle

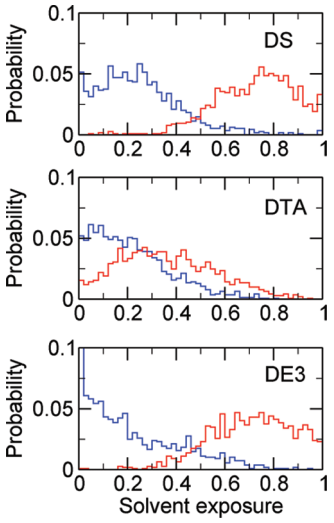

Figure 9. Probability distribution of the solvent exposure of the protonated (blue) and deprotonated (red) lauric acid from the explicit-solvent simulations. For definition for solvent exposure as well as other details see Figure 5.

panel of Figure 7 shows the RDFs from the carboxylate headgroup of protonated and deprotonated lauric acid to the counterions in the DS and DTA micelles. In the DS micelle, the RDF of sodium ions around the laurate ion shows two prominent peaks at 2.5 and 5 Å, reflecting the condensation of counterions, which is absent when lauric acid is protonated, as seen from the much weaker peaks in the RDF. In the DTA micelle, the distribution of counterions is qualitatively different, which is expected because chlorides have the same charge as the laurate ion. Due to electrostatic repulsion, the distance to the first RDF peak for the laurate ion is shifted relative to that for the lauric acid by 1.5 Å to 5 Å. The intensity of the peaks for both the lauric acid and laurate ion does not exceed the average density of chloride ions in the simulation box, suggesting the lack of ion condensation around the titrating lauric acid.

Distribution of Water Molecules around Lauric Acid. Solvation of the titrating lauric acid in explicit-solvent simulations can be studied by examining the RDF's of water molecules around the carboxylate headgroup (right panel of Figure 7). The shape of the RDFs is similar in all three micelles, with the first peak occurring at 3.5 Å. This peak is significantly enhanced for the laurate ion as compared to the lauric acid, a result of increased solvation for the former. To quantify solvation of lauric acid in the micelle, we calculated the average hydration number in the micelle and compare it with that in water. The hydration number is defined as the number of water molecules within a cutoff distance of 4.5 Å between the water oxygen and carboxylate carbon atoms (bottom center plot in Figure 7). 4.5 Å is the distance to the first minimum in the RDF of water distribution. Consistent with the RDF data, upon deprotonation of lauric acid, the hydration number significantly increases in all three micelles. As expected, upon transferring lauric acid from water to the micelle, the hydration number decreases for both protonated and deprotonated forms. For the neutral lauric acid the reduction in hydration is drastic, about 50%.

Position and Solvent Accessibility of Lauric Acid in the Micelle. We investigated the position and solvent accessibility of the titrating lauric acid in the three micelles. Figure 8 shows the probability distribution of the distances from the headgroups of lauric acid and surfactant monomers to the micellar center of mass. Figure 9 shows the relative solvent exposure of the carboxylate headgroup of lauric acid. In the DS micelle, the headgroup of the laurate ion explores similar positions as the DS headgroups, resulting in partial to full exposure to solvent. In contrast, the headgroup of the lauric acid explores similar space as the surfactant C1 atoms, consistent with partial to no solvent accessibility. This behavior is similar to the GB simulation.

In the DTA micelle, the headgroup of the lauric acid is on average closer to the micellar center as compared to the surfactant C1 atoms. Surprisingly, however, the maximum of the distribution for the laurate ion is also closer to the micellar center than that for the surfactant C1 atoms, although not as much as the lauric acid. Solvent exposure data reveals that the carboxylic acid group has very limited solvent accessibility similar to that in the DS micelle, while the carboxylate group explores states with zero to partial solvent exposure. This behavior is different from that in the GB simulation where the solvent accessibility for both protonated and deprotonated forms is very low (Table 2 and Figure 5), most likely due to the overly rigid micelle[35] which restricts the dynamics of the probe molecule.

The position and solvent accessibility of lauric acid in the DE3 micelle are similar to those in the DS micelle. The carboxylate carbon of the lauric acid explores similar positions as the C1 atom of DE3, having partial to no access to solvent. The carboxylate carbon of the laurate ion explores similar positions as the hydroxyl oxygen of DE3, resulting in full to partial access to solvent. A noticeable difference is that the neutral lauric acid spends more time in the fully buried position in the DE3 as compared to the DS micelle. The position and solvent accessibility of lauric acid offer an explanation for the trends observed in the average hydration numbers in three micelles. The average hydration number of the neutral lauric acid is the largest in the DS micelle because it has on average the largest solvent accessibility. It is worthwhile noting that the behavior of lauric acid in the DE3 micelle in the hybrid-solvent simulation is completely different from that in the GB simulation. In the latter, both the neutral and charged forms of lauric acid are deeply buried in the micellar core (Figure 4). As a result, the Born radii for the carboxylate oxygens in both charge states are much larger than those from the hybrid-solvent simulation (Table 2). Our previous work using the same GB model showed that solvent exposure of the hydrophilic headgroup of DE3 is reduced by as much as 80% relative to the hybrid-solvent simulation, while the reduction in solvation for the headgroups of DS and DTA is only 20−30%.[35] The lack of solvent dielectric screening promotes the formation of a hydrogen bond between the hydroxyl group of DE3 and the carboxylate of laurate ion. Such hydrogen bonding was not observed for the neutral carboxylic acid headgroup, likely because it is deeply buried in the hydrophobic core of the micelle, being farther away from the hydroxyl group of DE3. Overstabilization of hydrogen bonding is also a known deficiency in GB models. In protein folding simulations it manifests as the bias of helical vs extended conformations.[30,39] Despite the artificial conformational environment for both neutral and charged states of lauric acid, the calculated pK_a shift in the DE3 micelle is only 0.4 pK unit different from the hybrid-solvent simulation, which we believe is due to error cancellation, as the magnitude of both the desolvation and Coulombic terms is likely overestimated.

3.3. Qualitative Consideration of the pK_a Shifts in Micelles. The pK_a shift of a titratable probe in the micelle relative to the

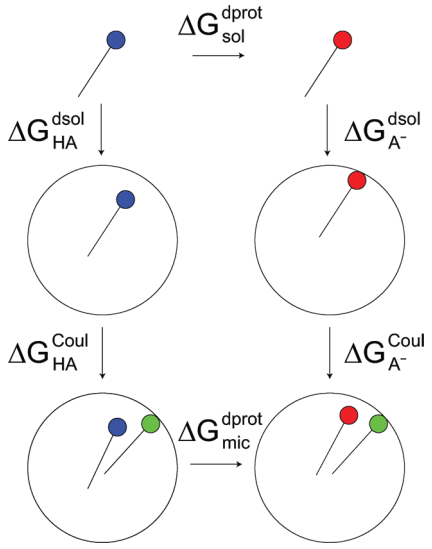

Figure 10. Thermodynamic cycle for the deprotonation of lauric acid in a positively charged micelle. Top, middle, and bottom represents lauric acid in water, neutral micelle, and charged micelle, respectively. Blue, red, and green spheres represent neutral, negatively charged, and positively charged headgroups, respectively.

solution value is the consequence of the change in the deprotonation free energy, $\Delta\Delta G^{\text{deprot}}$, when transferring the probe from water to the micellar environment

$$\Delta\Delta G^{\text{deprot}} = \Delta G^{\text{deprot}}_{\text{mic}} - \Delta G^{\text{deprot}}_{\text{sol}} = 2.3RT\Delta \text{p}K_a \qquad (5)$$

To help understand the sign of the pK_a shifts in micelles, we consider two hypothetical micelles with a solubilized surfactant probe consisting of an ionizable head and a nonpolar tail. The first micelle, which we refer to as the neutral micelle, is made up of molecules with a neutral polar head and a nonpolar tail. The second micelle, which we refer to as the charged micelle, is made up of molecules with a charged head and a nonpolar tail. The energetic contributions to the pK_a shift of the titratable surfactant can be now understood using a thermodynamic cycle as shown in Figure 10, which breaks down $\Delta\Delta G^{\text{deprot}}$ into desolvation and Coulombic terms

$$\Delta\Delta G^{\text{deprot}} = (\Delta G^{\text{dsol}}_{\text{A}^-} - \Delta G^{\text{dsol}}_{\text{HA}}) + (\Delta G^{\text{Coul}}_{\text{A}^-} - \Delta G^{\text{Coul}}_{\text{HA}})$$

$$= \Delta\Delta G^{\text{dsol}} + \Delta\Delta G^{\text{Coul}} \qquad (6)$$

Here the desolvation energy, $\Delta G^{\text{dsol}}_{\text{A}^-}$ or $\Delta G^{\text{dsol}}_{\text{HA}}$, refers to the free energy of transferring the deprotonated or protonated probe from solution to a neutral micelle. The Coulombic energy, $\Delta G^{\text{Coul}}_{\text{A}^-}$ or $\Delta G^{\text{Coul}}_{\text{HA}}$, refers to the electrostatic energy due to interaction with the charged surfactants in the micelle. The desolvation term, $\Delta\Delta G^{\text{dsol}}$, is defined as the difference in the desolvation energy between the ionized and neutral forms, while the Coulombic term, $\Delta\Delta G^{\text{Coul}}$, is defined as the difference in the Coulombic energy between the ionized and neutral forms.

Now we apply eq 6 to predict the sign of the pK_a shift of lauric acid in charged and neutral micelles. We first consider the sign of the desolvation and Coulombic terms. Since $\Delta G^{\text{dsol}}_{\text{A}^-}$ is always larger than $\Delta G^{\text{dsol}}_{\text{HA}}$, the desolvation term is always positive and contributes a positive pK_a shift via eq 5. The sign of the Coulombic term, however, varies. For a neutral micelle, although the sign of the Coulombic term is unclear, its magnitude is expected to be smaller than the desolvation term. Thus, the desolvation term dominates, predicting a positive pK_a shift for lauric acid. For a charged micelle, $\Delta G^{\text{Coul}}_{\text{A}^-}$ is always greater in magnitude than $\Delta G^{\text{Coul}}_{\text{HA}}$. If a micelle is negatively charged, due to electrostatic repulsion with laurate ion, $\Delta G^{\text{Coul}}_{\text{A}^-}$ is positive. Thus, the Coulombic term is positive, which together with the positive desolvation term results in a positive pK_a shift for lauric acid. If a micelle is positively charged, due to electrostatic attraction with laurate ion, $\Delta G^{\text{Coul}}_{\text{A}^-}$ is negative, which results in a negative Coulombic term. In this case, the sign of the pK_a shift depends on the balance between the Coulombic and desolvation terms. If the Coulombic term is greater in magnitude, a negative pK_a shift is expected. Conversely, if the desolvation term dominates, a positive pK_a shift results. It also follows that predicting the sign of the pK_a shift in a positively charged micelle is very challenging for methods based on microscopic energetics. Because of the cancellation of two large numbers, a small relative error can lead to a wrong direction of the calculated pK_a shift.

3.4. Microscopic Origins of the pK_a Shifts and Comparison to Experimental Data. It was observed in experiments that the pK_a of lauric acid shifts higher than the solution value when it is placed in the anionic DS and neutral DE3 micelles.[17,24] The positive pK_a shifts can be rationalized using a thermodynamic cycle which dissects the change in the deprotonation free energy upon transferring lauric acid from solution to micelle into desolvation and Coulombic terms. As compared to experiment, the calculated shifts based on our hybrid-solvent titration simulations are 0.4 units higher for the DS micelle and 0.2 units lower for the DE3 micelle. Microscopic data reveals that when lauric acid gains a proton in the DS and DE3 micelles, the carboxylate headgroup moves from the micelle surface toward the micelle hydrophobic interior. In the DS micelle, additional electrostatic repulsion between the laurate ion and DS monomers results in a positive Coulombic term, which contributes to a greater pK_a shift relative to the DE3 micelle. As salt concentration increases, the desolvation energy increases and Coulombic energy decreases according to eq 2. This is why the pK_a shift is increased by 0.2 units in the DE3 micelle when including 0.15 M salt in the simulation. Since the contribution from the Coulombic repulsion is larger than desolvation in the DS micelle, adding salt results in a decrease in the pK_a shift by 2.1 units.

What seemed puzzling and could not be reproduced with simplified continuum models[17] and thermodynamic theories[25] is the observed positive pK_a shifts of lauric acid in the cationic DTAC and DTAB micelles.[17,24] Also, intuition predicts a negative shift due to stabilization of the laurate ion by the DTA headgroups. Surprisingly, our hybrid-solvent data reveals that the positively charged DTA headgroups only show a slight preference for the ionized form of the lauric acid headgroup. Furthermore, the carboxylate headgroup samples both the micelle interior and surface regions with the solvent accessibility ranging from zero to full exposure. The latter observation may be attributed to the pronounced mobility of DTA monomers and large shape fluctuation of the micelle,[35] which, perhaps together with the increased distance between the headgroups of the laurate ion and DTA reduces the electrostatic attraction and hence the magnitude of the negative Coulombic term. On the other hand, partial burial of the laurate ion in the DTA micelle (relative to that in the DS and DE3 micelles) increases the desolvation energy. As a result, the hybrid-solvent titration gave a positive pK_a shift of 1.5 units. The balance between the

desolvation and Coulombic terms is also evident in the effects of salt screening. By including 0.15 M salt in the simulation, the pK_a shift in the DTA micelle is increased by 0.9 units, because of the greater desolvation and smaller Coulombic energies. One aspect that merits attention is the large difference between the measured pK_a shift in the DTAC and DTAB micelles.[17] In the presence of bromides, the pK_a shift is 0.9, 0.8 units higher than with chlorides,[17] which corroborates with the observation that DTAB has a smaller degree of micelle ionization,[54] perhaps due to tighter binding of bromides to the cationic micelle.[54,55] Binding of specific ions to the micelle reduces the net charge, resulting in a decreased attraction between the laurate ion and surfactant monomers. However, it is not straightforward to assess the magnitude relative to the effect due to mobile-ion screening which was accounted for in our simulations via the Debye−Hückel term. Nevertheless, we estimate the calculated pK_a shift for the DTA micelle to be in the range of 0.6−1.5. This is because ion binding increases the pK_a shift relative to the value of 0.6 calculated at zero ionic strength, while it also significantly reduces the shift relative to the value of 1.5 due to salt-screening effect. Interestingly, comparison of the experimental data for LiDS and SDS (Table 1) demonstrates that the nature of counterions has little impact on the titration of lauric acid in the anionic micelle. This is because the DS micelle is more hydrated than the DTA micelle such that ions are not directly bound to the DS headgroups.[55]

4. CONCLUDING REMARKS

We have performed GB and hybrid-solvent-based CpHMD titration simulations to calculate the pK_a shift of lauric acid in the anionic DS, cationic DTA, and nonionic DE3 micelles. The GB- and hybrid-solvent based titrations gave similar pK_a shifts for the DS and DE3 micelles, both of which are in good agreement with experiment. However, a large discrepancy was found for the DTA micelle, for which the GB simulation failed to predict the direction of the pK_a shift because of the undersolvation for the laurate ion, which resulted in a stronger electrostatic interaction with the DTA monomers than in the hybrid-solvent simulation. For the DE3 micelle, the good agreement with experiment in the GB simulation is due to error cancellation. Thus, our data demonstrates that ionization-coupled conformational dynamics and an accurate representation of the conformational environments of both protonated and deprotonated forms are crucial for quantitative prediction of the pK_a shifts in surfactant assemblies.

The present study also points out two limitations of the current hybrid-solvent based CpHMD technique. As seen in the titration data for the DTA micelle which undergoes a larger conformational fluctuation relative to the SD and DE3 micelles, while sampling of the protonation space is converged, the conformational equilibrium between the buried and interfacial states may not be fully reached due to the slow rate of conformational interconversion relative to the time scale of the simulation. The second limitation is related to the quantification of the effects due to counterion binding to the micelle. Experiment shows that the pK_a shift in the DTA micelle increases by as much as 0.8 units in the presence of bromides instead of chlorides. The Debye−Hückel approximation used in the current method, however, only accounts for the bulk dielectric screening effects due to mobile ions. Despite these limitations, the presented data is encouraging and demonstrates that hybrid-solvent CpHMD simulations based on conformational sampling in explicit solvent offer accurate calculation of micellar pK_a values and a microscopic view of ionization-coupled conformational dynamics, which is useful for understanding and formulating surfactant systems for a variety of applications.

■ ASSOCIATED CONTENT

Supporting Information. Cumulative unprotonated fractions versus time and additional fitting of the DTA titration curve for the hybrid-solvent simulations. This material is available free of charge via the Internet at http://pubs.acs.org.

■ AUTHOR INFORMATION

Corresponding Author

*Phone: (405) 325-0458. Fax: (405) 325-6111. E-mail: jana.k.shen@ou.edu.

■ ACKNOWLEDGMENT

We thank Procter & Gamble for financial support in the form of a corporate gift. Acknowledgment is also made to the Donors of American Chemical Society Petroleum Fund for partial support of this research. Some of the computing for this project was performed at the OU Supercomputing Center for Education & Research (OSCER) at the University of Oklahoma.

■ REFERENCES

(1) Tadros, T. F. *Applied Surfactants: Principles and Applications*; Wiley-VCH: Weinheim, Germany, 2005.
(2) Lindman, B.; Wennerström, H. In *Topics in Current Chemistry*; Boschke, F. L., Ed.; Springer-Verlag: Berlin, 1980; Vol. 87; Chapter Micelles Amphiphile Aggregation in Aqueous Solution, pp 8−90.
(3) Rosen, M. J. *Surfactants and Interfacial Phenomena*, 3rd ed.; Wiley-Interscience: Hoboken, NJ, 2004.
(4) Laughlin, R. G. *The Acqueous Phase Behaviour of Surfactants*; Academic Press: Sydney, 1994.
(5) Tanford, C. *J. Phys. Chem.* **1974**, *78*, 2469–2479.
(6) Nagarajan, R. *Langmuir* **1985**, *1*, 331–341.
(7) Nguyen, C. M.; Rathman, J. F.; Scamehorn, J. F. *J. Colloid Interface Sci.* **1986**, *112*, 438–445.
(8) Nagarajan, R.; Ruckenstein, E. *Langmuir* **1991**, *7*, 2934–2969.
(9) Puvvadat, S.; Blankschtein, D. *J. Phys. Chem.* **1992**, *96*, 5567–5579.
(10) Goldsipe, A.; Blankschtein, D. *Langmuir* **2007**, *23*, 5942–5952.
(11) Svenson, S. *Curr. Opin. Colloid Interface Sci.* **2004**, *9*, 201–212.
(12) Cistola, D. P.; Hamilton, J. A.; Jackson, D.; Small, D. M. *Biochemistry* **1988**, *27*, 1881–1888.
(13) Namani, T.; Walde, P. *Langmuir* **2005**, *21*, 6210–6219.
(14) Maeda, H.; Kakehashi, R. *Adv. Colloid Interface Sci.* **2000**, *88*, 275–293.
(15) Drummond, C. J.; Grieser, F.; Healy, T. W. *J. Phys. Chem.* **1988**, *92*, 2604–2613.
(16) Grieser, F.; Drummond, C. J. *J. Phys. Chem.* **1988**, *92*, 5580–5593.
(17) da Silva, F. L. B.; Bogren, D.; Söderman, O.; Åkesson, T.; Jönsson, B. *J. Phys. Chem. B* **2002**, *106*, 3515–3522.
(18) Mukerjee, P.; Banerjee, K. *J. Phys. Chem.* **1964**, *68*, 3567–3574.
(19) Fernández, M. S.; Fromherz, P. *J. Phys. Chem.* **1977**, *81*, 1755–1761.
(20) Mille, M. *J. Colloid Interface Sci.* **1981**, *81*, 169–179.
(21) Terada, Y.; Maeda, H.; Odagaki, T. *J. Phys. Chem. B* **1997**, *101*, 5784–5788.
(22) Maeda, H. *J. Colloid Interface Sci.* **2003**, *263*, 277–287.
(23) Goldsipe, A.; Blankschtein, D. *Langmuir* **2006**, *22*, 9894–9904.
(24) Söderman, O.; Jönsson, B.; Olofsson, G. *J. Phys. Chem. B* **2006**, *110*, 3288–3293.

(25) Goldsipe, A.; Blankschtein, D. *Langmuir* **2007**, *23*, 5953–5962.
(26) Lee, M. S.; Salsbury, F. R., Jr.; Brooks, C. L., III *Proteins* **2004**, *56*, 738–752.
(27) Khandogin, J.; Brooks, C. L., III *Biophys. J.* **2005**, *89*, 141–157.
(28) Im, W.; Lee, M. S.; Brooks, C. L., III *J. Comput. Chem.* **2003**, *24*, 1691–1702.
(29) Khandogin, J.; Brooks, C. L., III *Biochemistry* **2006**, *45*, 9363–9373.
(30) Khandogin, J.; Chen, J.; Brooks, C. L., III *Proc. Natl. Acad. Sci. U.S.A.* **2006**, *103*, 18546–18550.
(31) Khandogin, J.; Brooks, C. L., III *Proc. Natl. Acad. Sci. U.S.A.* **2007**, *104*, 16880–16885.
(32) Khandogin, J.; Raleigh, D. P.; Brooks, C. L., III *J. Am. Chem. Soc.* **2007**, *129*, 3056–3057.
(33) Wallace, J. A.; Shen, J. K. *Methods Enzymol.* **2009**, *466*, 455–475.
(34) Wallace, J. A.; Wang, Y.; Shi, C.; Pastoor, K. J.; Nguyen, B.-L.; Xia, K.; Shen, J. K. *Proteins* **2011**, *79*, 3364–3373.
(35) Wang, Y.; Wallace, J. A.; Koenig, P. H.; Shen, J. K. *J. Comput. Chem.* **2011**, *32*, 2348–2358.
(36) Wallace, J. A.; Shen, J. K. *J. Chem. Theory Comput.* **2011**, *7*, 2617–2629.
(37) Chen, J.; Brooks, C. L., III; Khandogin, J. *Curr. Opin. Struct. Biol.* **2008**, *18*, 140–148.
(38) Feig, M.; Onufriev, A.; Lee, M. S.; Im, W.; Case, D. A.; Brooks, C. L., III *J. Comput. Chem.* **2004**, *25*, 265–284.
(39) Shen, J. K. *Biophys. J.* **2010**, *99*, 924–932.
(40) Croonen, Y.; Geladé, E.; van der Zegel, M.; van der Auweraer, M.; Vandendriessche, H.; De Schryver, F. C.; Almgrent, M. *J. Phys. Chem.* **1983**, *87*, 1426–1431.
(41) Cabane, B.; Duplessix, R.; Zemb, T. *J. Phys. (Paris)* **1985**, *46*, 2161–2178.
(42) Alargova, R. G.; Kochijashky, I. I.; Sierra, M. L.; Zana, R. *Langmuir* **1998**, *14*, 5412–5418.
(43) Hansson, P.; Jonsson, B.; Strom, C.; Söderman, O. *J. Phys. Chem. B* **2000**, *104*, 3496–3506.
(44) MacKerell, A. D., Jr. *J. Phys. Chem.* **1995**, *99*, 1846–1855.
(45) Bruce, C. D.; Berkowitz, M. L.; Perera, L.; Forbes, M. D. E. *J. Phys. Chem. B* **2002**, *106*, 3788–3793.
(46) Brooks, B. R.; et al. *J. Comput. Chem.* **2009**, *30*, 1545–1614.
(47) Feller, S. E.; MacKerell, A. D., Jr. *J. Phys. Chem. B* **2000**, *104*, 7510–7515.
(48) Feller, S. E.; Gawrisch, K.; MacKerell, A. D., Jr. *J. Am. Chem. Soc.* **2002**, *124*, 318–326.
(49) Lee, H.; Venable, R. M.; MacKerell, A. D., Jr.; Pastor, R. W. *Biophys. J.* **2008**, *95*, 1590–1599.
(50) Jorgensen, W. L.; Chandrasekhar, J.; Madura, J. D.; Impey, R. W.; Klein, M. L. *J. Chem. Phys.* **1983**, *79*, 926–935.
(51) Jusufi, A.; Antti-Pekka, H.; Haataja, M.; Panagiotopoulos, A. Z. *J. Phys. Chem. B* **2009**, *113*, 6314–6320.
(52) Feig, M.; Karanicolas, J.; Brooks, C. L., III *J. Mol. Graph. Model.* **2004**, *22*, 377–395.
(53) Palaprat, G.; Ganachaud, F.; Mauzac, M.; Hémery, P. *Polymer* **2005**, *46*, 11213–11218.
(54) Sepúlveda, L.; Cortés, J. *J. Phys. Chem.* **1985**, *89*, 5322–5324.
(55) Buchner, R.; Baar, C.; Fernandez, P.; Schrödle, S.; Kunz, W. *J. Mol. Liq.* **2005**, *118*, 179–187.
(56) MacKerell, A. D., Jr.; et al. *J. Phys. Chem. B* **1998**, *102*, 3586–3616.